arXiv:2006.10761v2 [astro-ph.HE] 22 Jun 2020

ZTF20aajnksq (AT 2020blt): A Fast Optical Transient at $z \approx 2.9$ With No Detected Gamma-Ray Burst Counterpart

ANNA Y. Q. HO,[1] DANIEL A. PERLEY,[2] PAZ BENIAMINI,[1] S. BRADLEY CENKO,[3,4] S. R. KULKARNI,[1]
IGOR ANDREONI,[1] LEO P. SINGER,[3] KISHALAY DE,[1] MANSI M. KASLIWAL,[1] C. FREMLING,[1]
ERIC C. BELLM,[5] RICHARD DEKANY,[6] ALEXANDRE DELACROIX,[6] DMITRY A. DUEV,[1]
DANIEL A. GOLDSTEIN,[1,*] V. ZACH GOLKHOU,[5,7] ARIEL GOOBAR,[8] DAVID HALE,[6]
THOMAS KUPFER,[9] RUSS R. LAHER,[10] FRANK J. MASCI,[10] A. A. MILLER,[11,12] JAMES D. NEILL,[1]
REED RIDDLE,[6] BEN RUSHOLME,[10] DAVID L. SHUPE,[10] ROGER SMITH,[6] JESPER SOLLERMAN,[13] AND
JAN VAN ROESTEL[1]

[1]*Cahill Center for Astrophysics, California Institute of Technology, MC 249-17, 1200 E California Boulevard,
Pasadena, CA, 91125, USA*

[2]*Astrophysics Research Institute, Liverpool John Moores University, IC2, Liverpool Science Park, 146 Brownlow Hill,
Liverpool L3 5RF, UK*

[3]*Astrophysics Science Division, NASA Goddard Space Flight Center, Mail Code 661, Greenbelt, MD 20771, USA*

[4]*Joint Space-Science Institute, University of Maryland, College Park, MD 20742, USA*

[5]*DIRAC Institute, Department of Astronomy, University of Washington, 3910 15th Avenue NE, Seattle, WA 98195,
USA*

[6]*Caltech Optical Observatories, California Institute of Technology, Pasadena, CA 91125*

[7]*The eScience Institute, University of Washington, Seattle, WA 98195, USA*

[8]*The Oskar Klein Centre & Department of Physics, Stockholm University, AlbaNova, SE-106 91 Stockholm, Sweden*

[9]*Kavli Institute for Theoretical Physics, University of California, Santa Barbara, CA 93106, USA*

[10]*IPAC, California Institute of Technology, 1200 E. California Blvd, Pasadena, CA 91125, USA*

[11]*Center for Interdisciplinary Exploration and Research in Astrophysics (CIERA) and Department of Physics and
Astronomy, Northwestern University, 1800 Sherman Road, Evanston, IL 60201, USA*

[12]*The Adler Planetarium, Chicago, IL 60605, USA*

[13]*The Oskar Klein Centre & Department of Astronomy, Stockholm University, AlbaNova, SE-106 91 Stockholm,
Sweden*

Submitted to ApJ

ABSTRACT

We present ZTF20aajnksq (AT 2020blt), a fast-fading ($\Delta r = 2.4 \,\mathrm{mag}$ in $\Delta t = 1.3 \,\mathrm{d}$)
red ($g - r \approx 0.6 \,\mathrm{mag}$) and luminous ($M_{1626} = -25.9$) optical transient at $z = 2.9$
discovered by the Zwicky Transient Facility (ZTF). AT 2020blt shares several features
in common with afterglows to long-duration gamma-ray bursts (GRBs): (1) an optical
light curve well-described by a broken power-law with a break at $t_{\mathrm{j}} = 1 \,\mathrm{d}$ (observer-
frame); (2) a luminous ($L_X = 10^{46} \,\mathrm{erg\,s^{-1}}$) X-ray counterpart; and (3) luminous
($L_\nu = 4 \times 10^{31} \,\mathrm{erg\,s^{-1}\,Hz^{-1}}$ at $10 \,\mathrm{GHz}$) radio emission. However, no GRB was de-
tected in the $0.74 \,\mathrm{d}$ between the last ZTF non-detection ($r > 20.64$) and the first ZTF
detection ($r = 19.57$), with an upper limit on the isotropic-equivalent gamma-ray energy
release of $E_{\gamma,\mathrm{iso}} < 7 \times 10^{52} \,\mathrm{erg}$. AT 2020blt is thus the third afterglow-like transient dis-
covered without a detected GRB counterpart (after PTF11agg and ZTF19abvizsw) and

the second (after ZTF19abvizsw) with a redshift measurement. We conclude that the properties of AT 2020blt are consistent with a classical (initial Lorentz factor $\Gamma_0 \gtrsim 100$) on-axis GRB that was missed by high-energy satellites. Furthermore, by estimating the rate of transients with light curves similar to that of AT 2020blt in ZTF high-cadence data, we agree with previous results that there is no evidence for an afterglow-like phenomenon that is significantly more common than classical GRBs. We conclude by discussing the status and future of fast-transient searches in wide-field high-cadence optical surveys.

1. INTRODUCTION

Over the past half-century, thousands of long-duration gamma-ray bursts (GRBs; Piran 2004; Zhang & Mészáros 2004; Mészáros 2006; Kouveliotou et al. 2012) have been discovered by high-energy satellites. In the traditional GRB model, a collapsing massive star launches a collimated (opening angle $\theta_0 \approx 10°$) and ultrarelativistic (initial Lorentz factor $\Gamma_0 \gg 100$) outflow (MacFadyen & Woosley 1999) that tunnels through the stellar material and collides with the ambient medium, producing an "afterglow" across the electromagnetic spectrum (van Paradijs et al. 2000; Panaitescu & Kumar 2002).

Through follow-up observations of well-localized GRB triggers, hundreds of optical afterglows have been detected[1]. There are several reasons why optical surveys should also detect "orphan" afterglows, i.e. optical afterglows without associated GRBs. First, for an outflow with Lorentz factor Γ, relativistic beaming precludes the observer from seeing emission outside a cone of width $\theta = 1/\Gamma$. The outflow decelerates between the time of the GRB detection and the time of the optical afterglow detection, so the optical afterglow should be visible over a wider observing angle than the GRB (Rhoads 1997; Mészáros et al. 1998). Second, an outflow must entrain very little mass ($M_{ej} \approx 10^{-5}\,M_\odot$) to produce a GRB. If GRBs represent the extreme of a continuum of baryon-loading in relativistic jets, then "dirty fireballs" should exist, which would produce an afterglow but not a GRB (Dermer et al. 1999).

To discover orphan afterglows and dirty fireballs, surveys must be able to find afterglows without relying on a GRB trigger. Independently discovering optical afterglow emission is challenging because of the need for high-cadence observations over a wide field-of-view, as well as rapid follow-up. Furthermore, there is a formidable fog of more common fast-fading transients like stellar flares (Kulkarni & Rau 2006; Rau et al. 2008; Berger et al. 2013; Ho et al. 2018; van Roestel et al. 2019). Of the three optically discovered afterglows in the literature, two turned out to have associated classical GRBs: iPTF14yb (Cenko et al. 2015) was the counterpart to GRB 140226A, and ATLAS17aeu (Bhalerao et al. 2017; Stalder et al. 2017) was likely the counterpart to GRB 170105A.[2]

The first optically discovered afterglow, PTF11agg (Cenko et al. 2013), had no detected GRB counterpart. The redshift was constrained to be $1 < z < 2$, and Cenko et al. (2013) argued that it could represent the first dirty fireball. It has since become clear that the rate of such events is not significantly higher than the rate of classical GRBs (Cenko et al. 2015; Ho et al. 2018); the same conclusion was reached by Nakar & Piran (2003) based on X-ray afterglows. So, if dirty fireballs exist, they are either

---

[1] An up-to-date list is maintained at http://www.mpe.mpg.de/~jcg/grbgen.html

[2] The association is not fully secure, because the redshift of the afterglow was not measured.

rare or look significantly different from classical GRB afterglows.

Making the discovery of optical afterglows *routine* is one of the primary scientific goals of the Zwicky Transient Facility (ZTF; Graham et al. 2019; Bellm et al. 2019a) high-cadence surveys (Bellm et al. 2019b). To that end, we have devised a set of filters for identifying afterglow emission in real-time, and obtaining prompt follow-up observations to measure the redshift and any accompanying X-ray and radio emission. Here we describe the first afterglow detected as part of this effort, ZTF20aajnksq (AT 2020blt) at $z \approx 2.9$. Since then, we discovered a second afterglow: ZTF20abbiixp (AT 2020kym; Ho et al. 2020) turned out to be the afterglow to Fermi/LAT GRB 200524A (Yao et al in prep). In September 2019, ZTF also serendipitously discovered a cosmological afterglow (ZTF19abvizsw at $z = 1.26$; Burdge et al. 2019; Ho et al. 2019) in follow-up observations of gravitional-wave trigger S190901ap (Perley et al. in prep). Finally, ZTF detected the afterglow to GRB 190106A as ZTF19aabgebm; the detection was in low-cadence data and therefore the transient did not pass the fast-transient filter.

This paper is organized as follows. In §2 we present the discovery and follow-up observations of AT 2020blt. In §3 we model the outflow using the light curve and the spectral energy distribution (SED). We discuss possible interpretations in §4, and conclude that we cannot rule out the possibility that AT 2020blt was a classical GRB missed by high-energy detectors. We summarize and look to the future in §5.

2. OBSERVATIONS

2.1. *ZTF Discovery*

The ZTF Uniform Depth Survey (Goldstein et al. in prep) covers $2000 \, \mathrm{deg}^2$ twice per night in g-, r-, and i-band using the 48-inch Samuel Oschin Schmidt telescope at Palomar Observatory (P48). The ZTF observing system is described in Dekany et al. (2020). The pipeline for ZTF photometry makes use of the image subtraction algorithm of Zackay et al. (2016) and is described in Masci et al. (2019).

AT 2020blt was discovered at $r = 19.57 \pm 0.14 \, \mathrm{mag}$ (all magnitudes given in AB) in an image obtained on 2020 Jan 28.28[3], at the position $\alpha = 12^{\mathrm{h}}47^{\mathrm{m}}04.87^{\mathrm{s}}$, $\delta = +45^{\mathrm{d}}12^{\mathrm{m}}02.3^{\mathrm{s}}$ (J2000). One and a half hours later, the source had faded to $r = 20.01 \pm 0.16 \, \mathrm{mag}$.

AT 2020blt passed a filter that searches the ZTF alert stream (Patterson et al. 2019) for young and fast transients. More specifically, the filter identifies transients that:

- have an upper limit from the previous night that is at least one magnitude fainter than the first detection,

- have no historical detections in the Catalina Real-Time Transient Survey (Drake et al. 2009; Mahabal et al. 2011; Djorgovski et al. 2011), ZTF, or the predecessor to ZTF the Palomar Transient Factory (Law et al. 2009),

- have a real-bogus score `drb` > 0.9, which is associated with a false positive rate of 0.4% and a false negative rate of 5% (Duev et al. 2019),

- have two detections separated by at least half an hour (to remove asteroids), and

- have no stellar counterpart (`sgscore` < 0.76; Tachibana & Miller 2018)

AT 2020blt fulfilled the criteria listed above: the last upper limit from the high-cadence survey was 0.74 d prior to the first detection with an upper limit of $r > 20.73 \, \mathrm{mag}$. There is no source within $15''$ of the position of AT 2020blt in ZTF r-band and g-band reference images,

---

[3] All times in this paper are given in UTC.

with a 5-σ limiting magnitude in the PSF-fit reference image catalog of $r = 23.17$ mag and $g = 22.77$ mag.

Motivated by the fast rise and lack of a detected host galaxy counterpart in ZTF reference images (as expected for cosmological GRBs; the median magnitude of the TOUGH sample of 69 *Swift* GRB host galaxies (Hjorth et al. 2012) was $R = 25.52 \pm 0.23$ mag) we immediately triggered a series of follow-up observations (§2.2) which were coordinated through the GROWTH "Marshal" (Kasliwal et al. 2019). All observations will be made available on WISeREP, the Weizmann Interactive Supernova Data Repository (Yaron & Gal-Yam 2012).

2.2. *Follow-up Observations*
2.2.1. *Optical Imaging*

In searches for extragalactic fast transients, the primary false positives are stellar flares in the Milky Way (Kulkarni & Rau 2006; Rau et al. 2008; Berger et al. 2013; Ho et al. 2018). At optical frequencies, stellar flares can be distinguished from afterglow emission by color. At peak, stellar flares have typical blackbody temperatures of $\sim 10,000$ K (Kowalski et al. 2013), so optical filters will be on the Rayleigh-Jeans tail and colors will obey $f_\nu \propto \nu^{+2}$ ($g - r = -0.17$ mag). By contrast, in optical bands synchrotron emission obeys $f_\nu \propto \nu^{-0.7}$ or steeper (Sari et al. 1998), corresponding to $g - r \gtrsim 0.24$ mag (even without extinction). To measure the color of AT 2020blt, we triggered target-of-opportunity (ToO) programs on the IO:O imager of the Liverpool Telescope[4] (LT; Steele et al. 2004) and with the Spectral Energy Distribution Machine[5] (SEDM; Blagorodnova et al. 2018; Rigault et al. 2019) on the automated 60-inch telescope at Palomar Observatory (P60; Cenko et al. 2006). LT image reduction was

provided by the basic IO:O pipeline. P60 and LT image subtraction was performed following Fremling et al. (2016), using PS1 images for *griz* and SDSS for *u*-band.

LT *griz* observations on Jan 29.17 and P60 *gri* observations 3 hours later confirmed that AT 2020blt had red colors. Furthermore, forced photometry (Yao et al. 2019) on P48 images revealed two *g*-band detections that were below the 5-σ threshold of the nominal ZTF pipeline, which give $g - r = 0.79 \pm 0.16$ mag. Photometry was corrected for Milky Way extinction following Schlafly & Finkbeiner (2011) with $E(B - V) = A_V/R_V = 0.034$ mag, using $R_V = 3.1$ and a Fitzpatrick (1999) extinction law. The full light curve of AT 2020blt is shown in the left panel of Figure 1, and the photometry is listed in Table 1.

To monitor the light curve, we triggered a ToO program[6] with the Wafer-Scale Imager for Prime (WaSP) on the 200-inch Hale telescope at the Palomar Observatory (P200) and obtained 2×180 s exposures in each of *g*-, *r*-, and *i*-bands. The WaSP reductions were performed using a pipeline developed for Gattini-IR, described in De et al. (2020). The measurement established a rapid fade rate of 2.5 magnitudes in 1.25 days and confirmed the red colors ($g - r = 0.63 \pm 0.12$ mag).

For a final photometry measurement, we triggered a ToO observation with the Gemini Multi-Object Spectrograph (GMOS; Hook et al. 2004) on the Gemini-North 8-meter telescope on Mauna Kea[7]. In 8×200 s exposures on Feb 01.52, calibrating against PS1 DR1 (Chambers et al. 2016), we detected the source at $r = 25.20 \pm 0.05$ (Singer et al. 2020). Data were reduced using DRAGONS (Data Reduction for Astronomy from Gemini Observatory North and South), a Python-based reduction

---

[4] PI: D. Perley
[5] PI: A. Ho

[6] PI: I. Andreoni
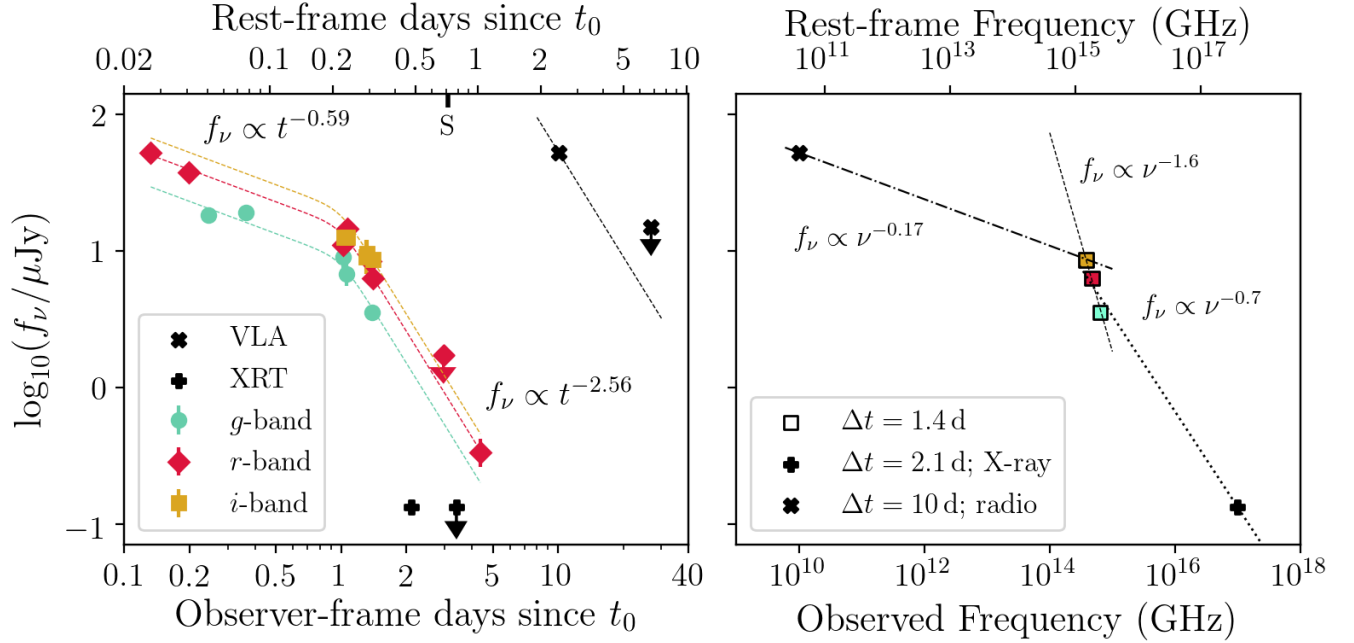[7] PI: L. Singer; Program ID GN-2019B-Q-130

Figure 1. Left: The optical (colored points), X-ray (black plus), and radio (black cross) light curves of AT 2020blt, shown in observer-frame days on the bottom x-axis and rest-frame days on the top x-axis. The X-ray and radio upper limits are at 3-σ. The estimated time of first light t_0=Jan 28.15 comes from fitting a broken power-law to the optical light curve (§3.1). The fitted function is shown as dashed lines. For the radio light curve, we show a dotted line with the same temporal index as the post-break optical light curve ($t^{-2.56}$). The 'S' along the top indicates the epoch of our LRIS spectrum. Right: the spectral energy distribution of AT 2020blt.

package provided by the Gemini Observatory. In §3.1 we model the full optical light curve of AT 2020blt and compare it to GRB afterglows in the literature.

2.3. *Optical Spectroscopy*

We triggered ToO observations[8] using the Low Resolution Imaging Spectrometer (LRIS; Oke et al. 1995) on the Keck I 10-m telescope. The observation details are listed in Table 1. The spectrum was reduced with `LPipe` (Perley 2019) and is shown in Figure 2. The spectrum showed features consistent with the Lyman break (rest-frame 912 Å) and Lyman-α absorption (rest-frame 1216 Å) at $z = 2.90^{+0.05}_{-0.04}$ (luminosity distance 25 Gpc[9]), although the S/N is low due to

the short exposure time and the fact that the observation started close to morning twilight. We searched for narrow lines consistent with $z = 2.9$ with no convincing detections. The redshift sets the rest-frame UV magnitude at the time of discovery as $M_{1626} = -25.91$ mag, assuming a distance modulus of 46.99 mag and a central wavelength of the ZTF r-band filter of 6340 Å.

2.4. *X-ray Observations*

We triggered ToO observations[10] with the X-Ray Telescope (XRT; Burrows et al. 2005) on board the Neil Gehrels *Swift* observatory (Gehrels et al. 2004). We obtained two epochs of 4 ks exposures and reduced the data us-

[8] PI: M. Kasliwal
[9] ΛCDM cosmology of Planck Collaboration et al. (2016) used throughout.

[10] PI: A. Ho, Target ID 13197

Table 1. Summary of observations of AT 2020blt. Time given relative to t_0 as defined in §3.1. Optical magnitudes have been corrected for Milky Way extinction. P48 values were measured using forced photometry (Yao et al. 2019). X-ray uncertainties are 1-σ and upper limits are 3-σ. Radio upper limits are 3× the image RMS. Uncertainties on radio measurements are given as the quadrature sum of the image RMS and a 5% uncertainty on the flux density due to flux calibration.

Optical Photometry				
Obs. Date	Δt (days)	Instrument	Filter	Mag
Jan 28.28	0.15	P48+ZTF	r	19.60 ± 0.08
Jan 28.35	0.18	P48+ZTF	r	19.97 ± 0.08
Jan 28.39	0.19	P48+ZTF	g	20.74 ± 0.14
Jan 28.51	0.31	P48+ZTF	g	20.70 ± 0.13
Jan 29.17	0.97	LT+IO:O	g	21.52 ± 0.21
Jan 29.17	0.97	LT+IO:O	r	21.29 ± 0.18
Jan 29.17	0.97	LT+IO:O	i	21.15 ± 0.25
Jan 29.17	0.97	LT+IO:O	z	20.82 ± 0.40
Jan 29.21	1.01	LT+IO:O	g	21.83 ± 0.21
Jan 29.21	1.01	LT+IO:O	r	21.00 ± 0.16
Jan 29.21	1.01	LT+IO:O	i	21.15 ± 0.27
Jan 29.45	1.25	P48+ZTF	i	21.52 ± 0.32
Jan 29.47	1.27	P48+ZTF	i	21.45 ± 0.25
Jan 29.51	1.31	P48+ZTF	r	21.58 ± 0.26
Jan 29.53	1.33	P200+WaSP	g	22.53 ± 0.10
Jan 29.55	1.35	P200+WaSP	r	21.90 ± 0.07
Jan 29.55	1.35	P200+WaSP	i	21.56 ± 0.05
Feb 01.53	4.33	Gemini-N+GMOS	r	25.09 ± 0.26

Optical Spectrum with LRIS on Keck-I			
Obs. Date	Δt (days)	Observing Setup	Exposure Time
Jan 30.64	2.44	1" slit, 400/3400 grism, 400/8500 grating, D560 dichroic	900 s

0.3–10 keV X-ray Observations with *Swift*/XRT			
Obs. Date	Δt (days)	Count Rate	Flux
Jan 29.70	2.1	$(3.96^{+1.30}_{-1.08}) \times 10^{-3}\,\mathrm{s}^{-1}$	$1.33^{+0.44}_{-0.36} \times 10^{-13}\,\mathrm{erg\,s^{-1}\,cm^{-2}}$
Jan 31.04	3.4	$< 3.95 \times 10^{-3}\,\mathrm{s}^{-1}$	$< 1.33 \times 10^{-13}\,\mathrm{erg\,s^{-1}\,cm^{-2}}$

VLA Radio Observations at 10 GHz				
Obs. Date	Δt	Time On-source	Flux Density	Flux at 10 GHz
Feb 07.24	9.96	0.7 hr	$52.1 \pm 6.5\,\mu\mathrm{Jy}$	$(5.21 \pm 0.65) \times 10^{-18}\,\mathrm{erg\,s^{-1}\,cm^{-2}}$
Feb 23.54	26.34	0.7 hr	$< 15\,\mu\mathrm{Jy}$	$< 1.5 \times 10^{-18}\,\mathrm{erg\,s^{-1}\,cm^{-2}}$
Apr 29.98	92.78	0.7 hr	$< 21\,\mu\mathrm{Jy}$	$< 2.1 \times 10^{-18}\,\mathrm{erg\,s^{-1}\,cm^{-2}}$

ing the online tool[11] developed by the *Swift* team (Evans et al. 2007). In the first epoch (Jan 29.70; $\Delta t = 2.1$ d) a source was detected at the position of AT 2020blt with a 0.3–10 keV count rate of $(3.96^{+1.30}_{-1.08}) \times 10^{-3}\,\mathrm{s}^{-1}$. Assuming a neutral hydrogen column density $n_H = 1.69 \times 10^{20}\,\mathrm{cm}^{-2}$ and a photon index $\Gamma = 2$ the unabsorbed flux density is $2.1^{+1.6}_{-1.2} \times 10^{-13}\,\mathrm{erg\,s^{-1}\,cm^{-2}}$. The source was not detected in the second epoch (Jan 31.04; $\Delta t = 3.4$ d)

with a 3-σ confidence upper limit of $< 4.57 \times 10^{-3}\,\mathrm{s}^{-1}$. We used `webpimms`[12] with $\Gamma = 2$ and the same value of n_H from the first observation to convert the upper limit on the count rate to an upper limit on the flux density of $< 1.57 \times 10^{-13}\,\mathrm{erg\,s^{-1}\,cm^{-2}}$. A log of our X-ray observations is provided in Table 1, and we model the X-ray to radio SED in §3.2.

2.5. *Radio Observations*

---

[11] https://www.swift.ac.uk/user_objects/

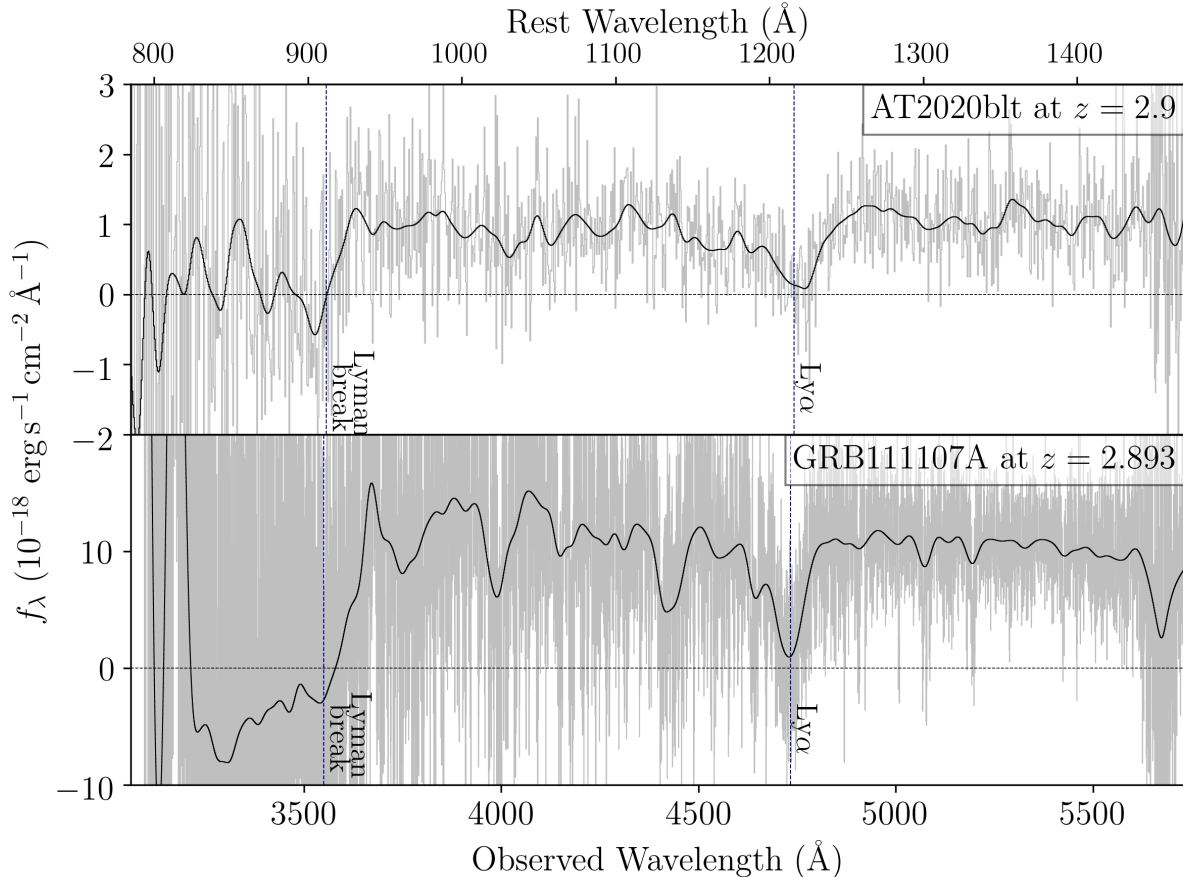[12] https://heasarc.gsfc.nasa.gov/cgi-bin/Tools/w3pimms/w3pimms.pl

Figure 2. Spectrum of AT 2020blt at $\Delta t = 2.4\,\mathrm{d}$ (top panel) with a spectrum of a GRB at a similar redshift in the literature for comparison (bottom panel). The spectrum of AT 2020blt was obtained with the blue arm of LRIS; there was negligible signal in the red arm. The spectrum of GRB 111107A is from Selsing et al. (2019). In each panel, the full spectrum is shown in grey and a smoothed spectrum is overplotted in black. The Lyman-α and Lyman break absorption features are marked with vertical dashed lines. We show $f_\lambda = 0$ with a horizontal dotted line.

On Feb 03 we triggered our ToO program on the Karl G. Jansky Very Large Array (VLA; Perley et al. 2011) for fast-rising and luminous transients[13]. We obtained an X-band observation on Feb 7.24 ($\Delta t = 9.96$) in C configuration, using 3C286 as the bandpass and flux density calibrator and J1219+4829 as the phase calibrator. We calibrated the data using the automated pipeline available in the Common Astronomy Software Applications (CASA; McMullin et al. 2007), and performed additional flagging manually before imaging. Imag-

ing was performed using the CLEAN algorithm (Högbom 1974) implemented in CASA. The cell size was 1/10 of the synthesized beamwidth, and the field size was the smallest magic number (10×2^n) larger than the number of cells needed to cover the primary beam. A source was detected at the position of AT 2020blt with a flux density of $47 \pm 5\,\mu\mathrm{Jy}$. In the next X-band image (Feb 24; $\Delta t \approx 27\,\mathrm{d}$) the source was not detected with an RMS of $5\,\mu\mathrm{Jy}$. In the final observation (Apr 29; $\Delta t \approx 92\,\mathrm{d}$) the source was not detected with an RMS of $7\,\mu\mathrm{Jy}$. A log of our radio observations is provided in Table 1. In §3.2 we model the X-ray to radio SED and in §3.3 we

---

[13] VLA/20A-374; PI: A. Ho

put the radio luminosity in the context of GRB afterglows.

2.6. *Search for Associated GRB*

The third Interplanetary Network (IPN[14]) consists of six spacecraft that provide all-sky full-time monitoring for high-energy bursts. The most sensitive detectors in the IPN are the *Swift* Burst Alert Telescope (BAT; Barthelmy et al. 2005) the *Fermi* Gamma-ray Burst Monitor (GBM; Meegan et al. 2009), and the Konus instrument on the WIND spacecraft (Aptekar et al. 1995).

We searched the *Fermi* GBM Burst Catalog[15], the *Fermi*-GBM Subthreshold Trigger list[16] (with reliability flag not equal to 2), the *Swift* GRB Archive[17], and the Gamma-Ray Coordinates Network archives[18] for an associated GRB between the last ZTF non-detection (Jan 27.54) and the first ZTF detection (Jan 28.28). There were no GRBs coincident with the position and time of AT 2020blt.[19]

The position of AT 2020blt was visible[20] to GBM only 65% of the time: 27% of the time it was occulted by the Earth, and 8% of the time GBM was not observing due to a South Atlantic Anomaly passage. By contrast, Konus-WIND is in interplanetary space, not Earth orbit, and therefore had complete coverage. Konus-WIND found no detection with a 90% confidence upper limit on the peak flux of $1.7 \times 10^{-7}\,\mathrm{erg\,cm^{-2}\,s^{-1}}$ for a typical long-GRB

---

[14] http://ssl.berkeley.edu/ipn3/index.html
[15] https://heasarc.gsfc.nasa.gov/W3Browse/fermi/fermigbrst.html
[16] https://gcn.gsfc.nasa.gov/fermi_gbm_subthresh_archive.html
[17] https://swift.gsfc.nasa.gov/archive/grb_table/
[18] https://gcn.gsfc.nasa.gov/gcn3_archive.html
[19] AT 2020blt was originally in the localization map of GRB 200128A because Earth occultation had not been taken into consideration (Hamburg & Fermi-GBM Team 2020).
[20] Search conducted using https://github.com/annayqho/HE_Burst_Search

spectrum[21] (Ridnaia et al. 2020). At the distance of AT 2020blt, this corresponds to an upper limit on the isotropic gamma-ray luminosity of $L_{\gamma,\mathrm{iso}} < 1.3 \times 10^{52}\,\mathrm{erg\,s^{-1}}$.

Overall, the IPN detects bursts with a 50–300 keV fluence of 1–$3\times10^{-6}\,\mathrm{erg\,cm^{-2}}$ at 50% efficiency. Following Cenko et al. (2013) we take $10^{-6}\,\mathrm{erg\,cm^{-2}}$ as a nominal fluence threshold and obtain a limit on the isotropic gamma-ray energy release of $E_{\gamma,\mathrm{iso}} < 7 \times 10^{52}\,\mathrm{erg}$. We put the limit on $E_{\gamma,\mathrm{iso}}$ in the context of classical GRBs in §3.

3. COMPARISON TO GRB AFTERGLOWS

AT 2020blt shares a number of features in common with classical GRBs in the literature. The redshift is typical of GRBs detected by *Swift* (Gehrels et al. 2009) and the absorption features seen in the spectrum are often seen in afterglows at these distances (Fynbo et al. 2009; Selsing et al. 2019). Given the low S/N of our spectrum we are not able to detect common metal lines at this redshift (e.g. C IV, Si IV) and we do not attempt to use the Ly-α absorption feature to measure the host hydrogen column density.

In Figure 3 we compare the X-ray, optical and radio luminosity of AT 2020blt to GRB afterglows (Nysewander et al. 2009; Chandra & Frail 2012), and show that a classical GRB cannot be ruled out based on the limit from Konus-WIND (in general, at cosmological redshifts Konus-WIND only detects the brightest GRBs). In the following sections we discuss the optical light curve and SED in more detail.

3.1. *Optical Light Curve*

As shown in Figure 1, the light curve of AT 2020blt has a clear break well-described by a broken power law. Optical afterglows with

---

[21] 20–1500 keV, 2.944 s scale, Band spectrum with $\alpha = 1, \beta = 2.5, E_p = 300\,\mathrm{keV}$
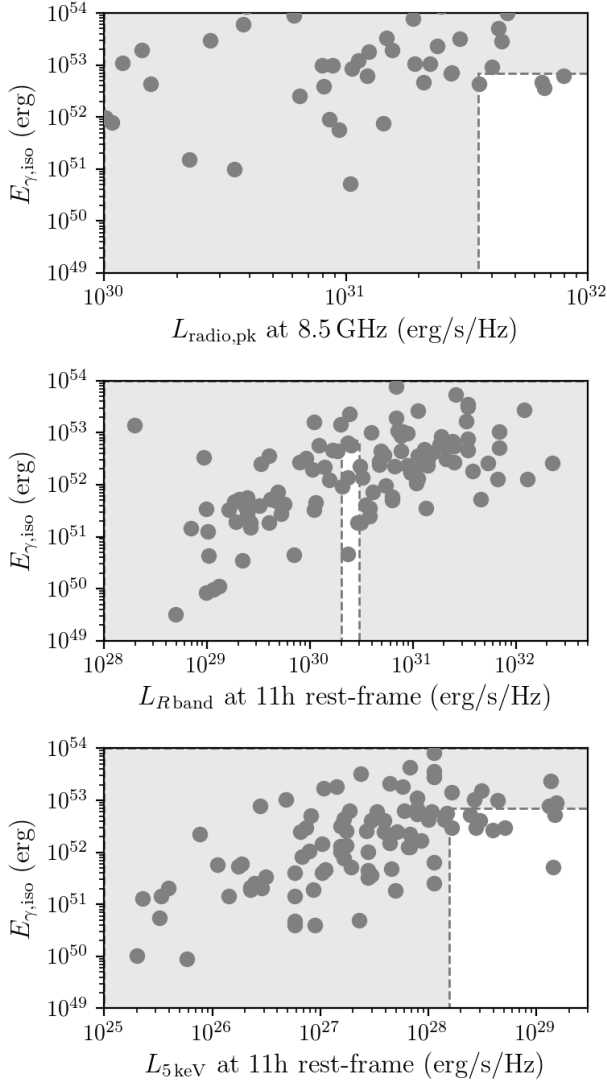
Figure 3. Optical, X-ray, and radio afterglow luminosity of classical GRB afterglows in the literature, compared to the isotropic gamma-ray energy release $E_{\gamma,\mathrm{iso}}$ (grey circles). The optical and X-ray afterglow values were taken from Figure 5 and Figure 6 of Nysewander et al. (2009), and the radio afterglow values were taken from Figure 20 of Chandra & Frail (2012). The region shaded in grey indicates the phase-space ruled out for AT 2020blt based on our observations and an upper limit on $E_{\gamma,\mathrm{iso}}$ from Konus-WIND. We cannot rule out the possibility that AT 2020blt was a classical GRB afterglow missed by high-energy detectors.

"classical" breaks like this were commonly observed prior to the *Swift* era (Kulkarni et al. 1999; Harrison et al. 2001; Klose et al. 2004; Zeh et al. 2006), so it was a surprise when relatively few such breaks were detected in the X-ray afterglows of *Swift* GRBs (Gehrels et al. 2009). Suggestions for why breaks are rarely detected include that observations do not extend long enough after the burst time (Dai et al. 2008), that the breaks are present in the data but missed in fitting (Curran et al. 2008), that bursts are viewed from a range of viewing angles (Zhang et al. 2015), and that *Swift* GRBs are on average more distant (Gehrels et al. 2009) and less energetic (Kocevski & Butler 2008). Furthermore, in X-ray as well as optical bands, the search for breaks can be complicated by the presence of flares or rebrightening episodes (e.g. Kann et al. 2010).

To make a direct comparison to afterglows in the literature with breaks (Zeh et al. 2006; Kann et al. 2010; Wang et al. 2018) we fit the light curve using a conventional smooth broken power law, modifying it to take into account the fact that we do not know the burst time t_0:

$$m(t) = -2.5 \log_{10} \left(
10^{-0.4 m_c} \left[\frac{(t - t_0)}{t_b}^{\alpha_1 n} + \frac{(t - t_0)}{t_b}^{\alpha_2 n} \right]^{-1/n} \right). \tag{1}$$

In Equation 1, $m(t)$ is the apparent magnitude as a function of time, n parameterizes the smoothness of the break (where $n = \infty$ is a sharp break), α_1 is the power-law index before the break, α_2 is the power-law index after the break, t_b is the time of the break, and m_c is the magnitude at the time of the break assuming $n = \infty$. Note that the original equation also includes terms for the underlying supernova and the host galaxy, which we take to be zero—a reasonable assumption given that we do not observe any flattening in the optical light curve.

First we fit Equation 1 to the r-band light curve, because it has the most extensive temporal coverage and we cannot necessarily assume constant colors across the optical light curve. Using the Levenberg-Marquardt algorithm implemented in `scipy` we find $m_c = 20.99 \pm 5.01$, $t_0 = 2458876.69 \pm 0.42$, $t_b = 1.00 \pm 1.84$ d, $\alpha_1 = 0.52 \pm 2.81$, $\alpha_2 = 2.59 \pm 0.26$, and a smoothing parameter that is very poorly constrained (large error bars). The fit has a reduced $\chi^2/\nu = 3.6/\nu$ where $\nu = 1$ is the number of degrees of freedom (number of data points minus number of fitted parameters).

In §2 we show that constant colors are a reasonable assumption at optical frequencies. So, to obtain more precise parameters we fit Equation 1 to the g-, r-, and i-band light curves simultaneously, assuming constant $g - r$ and $r - i$ offsets. The result is $m_c = 20.95 \pm 0.84$, $t_0 = 2458876.65 \pm 0.18$, $t_b = 1.00 \pm 0.43$ d, $\alpha_1 = 0.59 \pm 0.68$, and $\alpha_2 = 2.56 \pm 0.28$ (the smoothing parameter is still poorly constrained; $n = 5.54 \pm 14.2$). Note that we cannot assume a single spectral index across the optical band because the g-band flux is attenuated by the Ly-α absorption feature and the Lyman forest. The fit has a reduced $\chi^2/\nu = 11.8/\nu = 1.32$ where $\nu = 9$ is the number of degrees of freedom. Throughout the paper, we use the parameters resulting from the multi-band fit, which results in a best-fit light curve shown in the left panel of Figure 1.

The best-fit t_0 is Jan 28.15 ± 0.18, 3.1 hours before the first detection and 14.6 hours after the last non-detection. The best-fit $t_j = 1.00 \pm 0.43$ d after t_0 (observer-frame) is typical of optical afterglows with breaks (e.g. Zeh et al. 2006; Kann et al. 2010; Wang et al. 2018). In Figure 4 we show the resulting value of $\Delta\alpha = 1.97 \pm 0.74$ compared to the distribution in Zeh et al. (2006) and Kann et al. (2010). The value of $\Delta\alpha$ appears to be large compared to afterglows in the
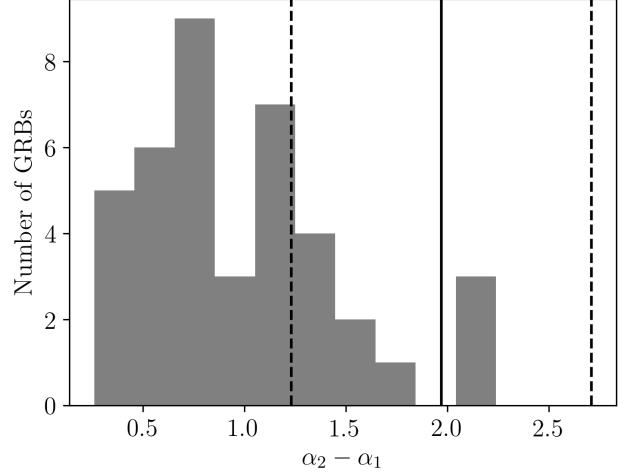
Figure 4. The difference between the post-break and pre-break temporal index, compared to a sample of GRBs with jet breaks from the literature (Zeh et al. 2006; Kann et al. 2010). The solid vertical line is the best-fit value of $\alpha_2 - \alpha_1$ from §3.1. The dashed vertical lines represent the error bars on the best-fit value.

literature, but given the uncertainties we cannot conclude that it is truly unusual.

The origin of breaks in afterglow light curves is still debated. A leading hypothesis is that a break results from a collimated jet (Rhoads 1997; Sari et al. 1999). The traditional argument is that while $\Gamma(t) \gg \theta^{-1}$, the emission cannot be distinguished from an isotropic outflow, because relativistic beaming confines the viewing angle to a small region that is expanding too quickly to interact sideways. As $\Gamma(t)$ decreases to $\Gamma(t) \sim \theta^{-1}$, two effects become important: the jet begins expanding sideways (Rhoads 1997), and the edge of the jet becomes visible (Mészáros & Rees 1999). However, "textbook" achromatic breaks are rarely observed, and simulations suggest that breaks can be chromatic (van Eerten et al. 2011) and that sideways expansion can take place significantly later than when the edge of the jet becomes visible (Panaitescu et al. 1998; Granot & Piran 2012).

If the break in the light curve of AT 2020blt is a jet break — and we caution that it is rare to see breaks that actually behave in the way one would expect for jet breaks, e.g. Liang et al. (2008) — we can use the timing of the break to estimate the opening angle of the jet θ_0. For a constant-density ISM we have from Sari et al. (1999) that

$$t_{\mathrm{jet}} \approx 6.2(E_{52}/n_1)^{1/3}(\theta_0/0.1)^{8/3}\,\mathrm{hr} \qquad (2)$$

where E_{52} is the kinetic energy release of the explosion in units of $10^{52}\,\mathrm{erg}$, θ_0 is in radians, and n_1 is the ambient density in units $1\,\mathrm{cm}^{-3}$. Using our rest-frame value $t_{\mathrm{jet}} = 0.26 \pm 0.11\,\mathrm{d}$ ($6.24 \pm 2.64\,\mathrm{hr}$) we have

$$1.0 \pm 0.4 = (E_{52}/n_1)^{1/3}(\theta_0/0.1)^{8/3}\,\mathrm{hr}. \qquad (3)$$

We do not have an independent constraint on E_{52} and n_1, but the E_{52}/n_1 term has a much weaker dependence than the opening angle term. Taking (E_{52}/n_1) to be unity, we find an opening angle of $\theta_0 = 0.10 \pm 0.07 = 5.7 \pm 4.0\,\mathrm{degrees}$, typical of opening angles inferred from optical jet breaks (Panaitescu & Kumar 2001; Zeh et al. 2006; Wang et al. 2018).

If the break is due to the material spreading sideways, then the temporal index after the break is $F_\nu(t) \propto t^{-p}$ (Sari et al. 1999) where p is the power-law index of the electron energy distribution. Using the value of α_2 above we have $p = \alpha_2 = 2.9 \pm 0.4$, which is large but consistent with values expected for shock acceleration (Jones & Ellison 1991) given the uncertainties, and furthermore is within the normal range of values inferred from optical afterglows in the literature (Wang et al. 2018).

If the steepening is due solely to detecting the edge of the jet, the expected post-break slope[22] is the slope of a spherically expanding outflow

---

[22] Here we assume that the optical frequency ν is in the regime $\nu_m < \nu < \nu_c$, motivated in §3.2 and §3.3.

($t^{-3(p-1)/4}$; Sari et al. 1999) with two additional powers of $\Gamma \propto t^{-3/8}$. The resulting temporal slope is $F_\nu(t) \propto t^{-3p/4}$, so $3p/4 = \alpha_2 = 2.9 \pm 0.4$. The value of $p = 3.9 \pm 0.5$ is larger than what is predicted for shock acceleration (Jones & Ellison 1991) so in what follows we assume $p = 2.9 \pm 0.4$.

3.2. Spectral Energy Distribution

The spectrum of an afterglow is determined by the kinetic energy of the explosion, the ambient density, and the fraction of the energy in magnetic fields ϵ_B and relativistic electrons ϵ_e (Sari et al. 1998). The spectrum is characterized by several break frequencies: the cooling frequency ν_c, the characteristic frequency ν_m, and the self-absorption frequency ν_a. The spectral index in any region of the spectrum therefore depends on physical properties of the explosion and on the position of the observing frequency relative to the break frequencies.

In §3.1 we found $p = 2.9 \pm 0.4$ based on the post-break light curve power-law index. Because the g-band measurement is attenuated by Lyman-α and Lyman forest absorption, we use the $r - i$ color from the WASP observation ($r - i = 0.34 \pm 0.09\,\mathrm{mag}$) to estimate that the optical spectral index $\beta_{\mathrm{opt}} = 1.5 \pm 0.4$. Such a steep spectral index is only ever observed as a result of absorption (Cenko et al. 2009; Greiner et al. 2011): at this redshift even i-band is well into the far-ultraviolet, so it takes relatively little extinction to significantly alter the flux and color. If β_{opt} were the "true" (unextincted) spectral index, that would indicate that the cooling frequency ν_c lies below the optical bands (Sari et al. 1999). Taking $\nu_c < 10^{14}\,\mathrm{Hz}$ at $t_d \approx 0.5\,\mathrm{d}$ we have, following Sari et al. (1998)

$$26 > \epsilon_B^{-3/2} E_{52}^{-1/2} n_1^{-1}. \qquad (4)$$

Using $\epsilon_B < 3 \times 10^{-4}$ and $E_{52} = 1$ (§3.3) we find a very large CSM density of $n > 7 \times 10^3\,\mathrm{cm}^{-3}$. Furthermore, as shown in the right panel of Fig-

ure [1], the optical to X-ray spectral index is $\beta_{\text{opt},X} \approx 0.7$, inconsistent with β_{opt}. It seems natural that the optical spectral index is steepened by dust attenuation, and $\beta_{\text{opt},X}$ is the "true" spectral index.

The value of $\beta_{\text{opt},X}$ is consistent with $(p-1)/2$ but not with $p/2$, so the cooling frequency ν_c lies above the X-ray band (Sari et al. 1999). For adiabatic evolution we have (Sari et al. 1998)

$$\nu_c = 2.7 \times 10^{12} \epsilon_B^{-3/2} E_{52}^{-1/2} n_1^{-1} t_d^{-1/2} \, \text{Hz}. \quad (5)$$

where t_d is the time (in days) after the explosion. Taking $\nu_c > 10^{18}$ Hz and $t_d = 0.5$ d (time of the X-ray observation; rest-frame), we have

$$2.6 \times 10^5 < \epsilon_B^{-3/2} E_{52}^{-1/2} n_1^{-1}. \quad (6)$$

Using $\epsilon_B < 3 \times 10^{-4}$ and $E_{52} = 1$ (§3.3) we find $n < 0.7 \, \text{cm}^{-3}$, which is typical for GRBs (Panaitescu & Kumar 2001; Chandra & Frail 2012).

3.3. Radio Light Curve

In §3.1 we showed that the optical light curve of AT 2020blt is fairly typical for classical GRBs. However, In the radio light curve of AT 2020blt (left panel of Figure 1) we detect a decay steeper than $F_\nu \propto t^{-2.3}$, which is unusual for GRBs with detected radio afterglows in general (Chandra & Frail 2012), including PTF11agg (Cenko et al. 2013).

Early fast-evolving emission in GRB radio afterglow light curves can arise from reverse shocks or diffractive scintillation in the interstellar medium (Laskar et al. 2013; Perley et al. 2014; Laskar et al. 2016; Alexander et al. 2017; Laskar et al. 2018; Alexander et al. 2019). To determine whether scintillation could be the origin in this case, we use the NE2001 model of the ISM (Cordes & Lazio 2002). For context, scintillation results from small-scale inhomogeneities in the ISM, which change the phase of an incoming wavefront. As the Earth moves,

the line of sight to a background source changes, so the net effect is an observed change in flux. The effect is greatest for sources observed at a frequency ν_{obs} that is close to the transition frequency ν_0, which separates strong scattering ($\nu_{\text{obs}} < \nu_0$) from weak scattering ($\nu_{\text{obs}} > \nu_0$).

Using the NE2001 map, we determine that the line-of-sight towards AT 2020blt has a transition frequency $\nu_0 = 7.12 \, \text{GHz}$, which is close to our observing frequency. Furthermore, we can estimate the timescale for flux changes. Using $D = 100 \, \text{pc}$ as the characteristic scale height of the ISM, and $\lambda = 3 \, \text{cm}$ as our observing wavelength, the Fresnel length is $r_f = \sqrt{\lambda D} \approx 10^{10} \, \text{cm}$. Assuming that Earth moves at $v = 30 \, \text{km s}^{-1}$, we obtain $t \sim r_f/v \approx 1 \, \text{hr}$. In conclusion, the flux could easily change by an order of magnitude due to scintillation over the large time window (16 d) between our observations. Note that the timescale is close to our time on-source (~ 30 minutes), so there could be some damping of the scintillation over the course of our observation. However, the signal-to-noise of the data is not high enough for us to search for scintillation within the observation.

If, on the other hand, the rapid change in flux is due to a truly steep power-law decay in the radio emission, there would be implications for the ambient density and the value of ϵ_B. In particular, the characteristic frequency ν_m must lie below the radio band. For adiabatic evolution we have (Sari et al. 1998)

$$\nu_m = 5.7 \times 10^{14} \epsilon_B^{1/2} \epsilon_e^2 E_{52}^{1/2} t_d^{-3/2} \, \text{Hz}. \quad (7)$$

Requiring $\nu_m < 10 \, \text{GHz}$ (39 GHz rest-frame) at $t_d = 2 \, \text{d}$ (time of the radio detection; rest-frame) and adopting $\epsilon_e = 0.1$ (Kumar & Zhang 2015; Beniamini & van der Horst 2017) we find

$$0.02 > \epsilon_B^{1/2} E_{52}^{1/2}. \quad (8)$$

Assuming $E_{52} = 1$, we find $\epsilon_B < 3 \times 10^{-4}$, which is also typical for GRBs based on high-energy and optical afterglow modeling (Kumar

& Zhang 2015; Beniamini & van der Horst 2017). So, although an early steep-decaying radio light curve is unusual for GRBs with detailed radio observations, we have no reason to believe that the radio behavior of AT 2020blt is unusual for the population of GRBs as a whole.

4. INTERPRETATION

In §3 we found that the optical and radio light curve of AT 2020blt is similar to that of classical GRB afterglows. The fact that we observed an achromatic steepening suggests that there was a jet break, which requires that our observing angle was within the jet opening angle.

Three possibilities remain for the origin of AT 2020blt. The first (and simplest) possibility is that AT 2020blt was a classical GRB viewed directly on-axis ($\theta_{\rm obs} < \theta_0$) for which the high-energy emission was simply missed by GRB satellites. As discussed in §3, the on-axis scenario is entirely possible. With an eye to the future, when larger samples of optical afterglows will be available (including some with more stringent limits on associated GRB emission), we consider two additional possibilities: that AT 2020blt is a classical GRB observed slightly off-axis $\theta_{\rm obs} \gtrsim \theta_0$ (§4.1) and that AT 2020blt is a dirty fireball (§4.2).

4.1. A Slightly Off-Axis GRB

Here we consider the possibility that AT 2020blt was a classical GRB viewed slightly outside the jet opening angle. Beniamini & Nakar (2019) argued that the vast majority of GRBs observed so far must have been observed close to or within the jet core, implying that GRB emission is not produced efficiently away from the core. So, as discussed in §1, there is a natural expectation for X-ray and optical afterglows without detected GRB emission (Mészáros & Rees 1997; Rhoads 1997; Nakar & Piran 2003). The slightly off-axis model has been invoked to explain low-luminosity GRBs or X-ray flashes (Ramirez-Ruiz et al. 2005) as

well as plateaus observed in X-ray afterglow light curves (Eichler & Granot 2006; Beniamini et al. 2020a).

One signature of a slightly off-axis afterglow could be an early shallow decay and a large value of $\Delta\alpha$ (Ryan et al. 2019; Beniamini et al. 2020b). This can be understood as follows. In on-axis events, the early stage of the light curve is set by two competing effects: the shock is decelerating, but the beaming cone is widening to include more material. In a slightly off-axis event, there is a third effect, which is that the beaming cone widens to include material of increasing energy per solid angle—hence a shallower decay.

A larger number of events would help to test this hypothesis: the luminosity function of the early afterglow should be different from the luminosity function of directly on-axis afterglows, and the distribution of limits on $E_{\rm iso}$ would eventually make it unlikely that the afterglows are drawn from the same population as classical GRBs. With more events, we could hope to make the first measurement of the optical beaming factor in GRB afterglows (Nakar & Piran 2003).

4.2. A Dirty Fireball

Here we consider the possibility that AT 2020blt was a "dirty fireball," i.e. a jet with lower Lorentz factor ($\Gamma \sim 10$) that did not produce any GRB emission, as proposed for PTF11agg (Cenko et al. 2013). The basis for the dirty fireball argument for PTF11agg was the rate: at the time, it seemed that the rate of PTF11agg-like events may have been significantly higher than the rate of classical GRBs (Cenko et al. 2013), although this was later shown to not be the case (Cenko et al. 2015; Ho et al. 2018). Taking a similar approach to Cenko et al. (2015) and Ho et al. (2018), we searched high-cadence (6×/night) ZTF survey data (Bellm et al. 2019b) from 2018 March 1 to 2020 May 12 to estimate the areal exposure

in which an event like AT 2020blt would have passed our filter.

We folded the light curve of AT 2020blt through all r-band exposures in the ZTF high-cadence fields, varying the burst time by 0.01 d intervals, to see over what duration the transient would have had two r-band detections above the limiting magnitude, with a first detection over one magnitude brighter than the last non-detection. We found a total exposure of 855 field-nights. We assume a 100% detection efficiency, so our result is somewhat of a lower limit, particularly at these fainter magnitudes; the efficiency as a function of limiting magnitude has not yet been characterized for ZTF. The 92 high-cadence survey fields included in our search have a combined footprint of 3307 deg² after removing the overlap between fields. So, we estimate the all-sky rate of transients similar to AT 2020blt to be

$$
\begin{aligned}
\mathcal{R} &\equiv \frac{N_{\rm rel}}{A_{\rm eff}} \\
&= \frac{1}{30{,}734\,{\rm deg}^2\,{\rm d}} \times \frac{365.25\,{\rm d}}{\rm year} \times \frac{41{,}253\,{\rm deg}^2}{\rm sky} \\
&= 490\,{\rm yr}^{-1}
\end{aligned}
\tag{9}
$$

with a 68% confidence interval from Poisson statistics of 85–1611 yr^{-1}. For comparison, the all-sky rate of *Swift* GRBs out to $z = 3$ has been estimated to be 1455^{+80}_{-112} yr^{-1} (Lien et al. 2014). The *Swift* GRB rate is larger than the rate of optical afterglows, since only a subset of GRBs show bright optical afterglow emission (Cenko et al. 2009). So, within the uncertainties, the rate of optical afterglows in ZTF is compatible with the GRB rate. We therefore concur with the conclusion in Cenko et al. (2015) and Ho et al. (2018) that there is no evidence for an afterglow-like phenomenon that is significantly more common than classical GRBs.

Of course, this assumes that a dirty fireball would look like a classical optical afterglow. We caution, however, that the light curve of a dirty fireball should take longer to rise to peak. The rise time of an afterglow is the time it takes the shock to sweep up material of mass $1/\Gamma_0$ times the ejecta mass (the "deceleration" time). For a uniform-density medium, the expression (observer-frame) is

$$
t_{\rm dec} = 30\,E_{53}^{1/3}n^{-1/3}\Gamma_{0,2.5}^{-8/3}\ {\rm sec}\,.
\tag{10}
$$

So, an outflow with $\Gamma_0 = 100$ will have an afterglow that rises to peak in 300 s, but an outflow with $\Gamma_0 = 10$ will have an afterglow that rises to peak in 1.2 d. We have no evidence for such a long rise time in AT 2020blt; the last non-detection was 0.74 d prior to the first detection. A slower-rising event might not pass our fast-transient filter (§2) so the limit we set on the rate would not be correct, i.e. the rate could be larger.

5. SUMMARY AND CONCLUSIONS

To summarize, we used a filter for extragalactic fast transients together with fast-turnaround follow-up observations to discover a cosmological afterglow ($z \approx 2.9$) in ZTF high-cadence data. Our search strategy (§2.1) is to find fast-appearing transients with no host galaxy and red colors, inconsistent with the thermal emission expected for the foreground fog of stellar flares. Additional photometry obtained within 24 hours confirmed rapid fading, and a spectrum obtained within three days established the cosmological origin (§2.2). AT 2020blt is one of only a few optical afterglows discovered independently of a high-energy trigger, and one of only two events with both a redshift measurement and no detected GRB.

One lesson from our work is that for a single event, it is very difficult to rule out a classical GRB missed by high-energy detectors. The most sensitive detectors have the smallest probability of observing the field over the relevant

time interval, given the typical cadence of optical observations.

We consider what might be possible with a large sample of events. From existing survey data, it is already clear that the rate of afterglow-like events cannot be significantly higher than the rates of classical GRBs (§4). Dirty fireballs could have a significantly longer duration (§4.2), in which case they would not pass our fast-transient filter and the rate could be significantly higher than the limits set by intra-night fast-transient searches. The appearance of slightly off-axis events (§4.1) depends on the structure of the jet, currently unknown, but the luminosity function should be different (with lower overall luminosity) than that of classical GRBs.

Perhaps the strategy of searching for intra-night transients is too restrictive, given the likelihood that dirty fireballs would be longer-duration transients and the uncertainty in the appearance of a slightly off-axis jet. A more agnostic strategy could be to search for relativistic explosions on the basis of luminosity. If dirty fireballs have an intrinsically lower redshift distribution, then their host galaxies are more likely to be detected; in fact, of the three afterglows with ZTF detections, two (ZTF19aabgebm and ZTF19abvizsw) have detected host galaxies in the Legacy Survey DR8 (Dey et al. 2019) with high photometric redshifts. In a search for luminous transients, interlopers like superluminous supernovae could be easily ruled out by light-curve duration. A search for luminous transients using host-galaxy photometric and spectroscopic catalogs during ZTF Phase II could help set the stage for a similar search strategy during LSST.

Facilities: Swift, EVLA, VLA, Liverpool:2m, PO:1.2m, PO:1.5m

Software: CASA, astropy, matplotlib, scipy, DRAGONS

REFERENCES

Alexander, K. D., Laskar, T., Berger, E., et al. 2017, ApJ, 848, 69, doi: 10.3847/1538-4357/aa8a76

—. 2019, ApJ, 870, 67, doi: 10.3847/1538-4357/aaf19d

Aptekar, R. L., Frederiks, D. D., Golenetskii, S. V., et al. 1995, SSRv, 71, 265, doi: 10.1007/BF00751332

Barthelmy, S. D., Barbier, L. M., Cummings, J. R., et al. 2005, SSRv, 120, 143, doi: 10.1007/s11214-005-5096-3

Bellm, E. C., Kulkarni, S. R., Graham, M. J., et al. 2019a, PASP, 131, 018002, doi: 10.1088/1538-3873/aaecbe

Bellm, E. C., Kulkarni, S. R., Barlow, T., et al. 2019b, PASP, 131, 068003, doi: 10.1088/1538-3873/ab0c2a

Beniamini, P., Duque, R., Daigne, F., & Mochkovitch, R. 2020a, MNRAS, 492, 2847, doi: 10.1093/mnras/staa070

Beniamini, P., Granot, J., & Gill, R. 2020b, MNRAS, 493, 3521, doi: 10.1093/mnras/staa538

Beniamini, P., & Nakar, E. 2019, MNRAS, 482, 5430, doi: 10.1093/mnras/sty3110

Beniamini, P., & van der Horst, A. J. 2017, MNRAS, 472, 3161, doi: 10.1093/mnras/stx2203

Berger, E., Leibler, C. N., Chornock, R., et al. 2013, ApJ, 779, 18, doi: 10.1088/0004-637X/779/1/18

Bhalerao, V., Kasliwal, M. M., Bhattacharya, D., et al. 2017, ApJ, 845, 152, doi: 10.3847/1538-4357/aa81d2

Blagorodnova, N., Neill, J. D., Walters, R., et al. 2018, PASP, 130, 035003, doi: 10.1088/1538-3873/aaa53f

Burdge, K., Perley, D. A., Kasliwal, M. M., & Growth Collaboration. 2019, GRB Coordinates Network, 25639, 1

Burrows, D. N., Hill, J. E., Nousek, J. A., et al. 2005, SSRv, 120, 165, doi: 10.1007/s11214-005-5097-2

Cenko, S. B., Fox, D. B., Moon, D.-S., et al. 2006, PASP, 118, 1396, doi: 10.1086/508366

Cenko, S. B., Kelemen, J., Harrison, F. A., et al. 2009, ApJ, 693, 1484, doi: 10.1088/0004-637X/693/2/1484

Cenko, S. B., Kulkarni, S. R., Horesh, A., et al. 2013, ApJ, 769, 130, doi: 10.1088/0004-637X/769/2/130

Cenko, S. B., Urban, A. L., Perley, D. A., et al. 2015, ApJL, 803, L24, doi: 10.1088/2041-8205/803/2/L24

Chambers, K. C., Magnier, E. A., Metcalfe, N., et al. 2016, arXiv e-prints, arXiv:1612.05560. https://arxiv.org/abs/1612.05560

Chandra, P., & Frail, D. A. 2012, ApJ, 746, 156, doi: 10.1088/0004-637X/746/2/156

Cordes, J. M., & Lazio, T. J. W. 2002, arXiv e-prints, astro. https://arxiv.org/abs/astro-ph/0207156

Curran, P. A., van der Horst, A. J., & Wijers, R. A. M. J. 2008, MNRAS, 386, 859, doi: 10.1111/j.1365-2966.2008.13043.x

Dai, X., Garnavich, P. M., Prieto, J. L., et al. 2008, ApJL, 682, L77, doi: 10.1086/591041

De, K., Hankins, M. J., Kasliwal, M. M., et al. 2020, PASP, 132, 025001, doi: 10.1088/1538-3873/ab6069

Dekany, R., Smith, R. M., Riddle, R., et al. 2020, PASP, 132, 038001, doi: 10.1088/1538-3873/ab4ca2

Dermer, C. D., Chiang, J., & Böttcher, M. 1999, ApJ, 513, 656, doi: 10.1086/306871

Dey, A., Schlegel, D. J., Lang, D., et al. 2019, AJ, 157, 168, doi: 10.3847/1538-3881/ab089d

Djorgovski, S. G., Drake, A. J., Mahabal, A. A., et al. 2011, arXiv e-prints, arXiv:1102.5004. https://arxiv.org/abs/1102.5004

Drake, A. J., Djorgovski, S. G., Mahabal, A., et al. 2009, ApJ, 696, 870, doi: 10.1088/0004-637X/696/1/870

Duev, D. A., Mahabal, A., Masci, F. J., et al. 2019, MNRAS, 489, 3582, doi: 10.1093/mnras/stz2357

Eichler, D., & Granot, J. 2006, ApJL, 641, L5, doi: 10.1086/503667

Evans, P. A., Beardmore, A. P., Page, K. L., et al. 2007, A&A, 469, 379, doi: 10.1051/0004-6361:20077530

Fitzpatrick, E. L. 1999, PASP, 111, 63, doi: 10.1086/316293

Fremling, C., Sollerman, J., Taddia, F., et al. 2016, A&A, 593, A68, doi: 10.1051/0004-6361/201628275

Fynbo, J. P. U., Jakobsson, P., Prochaska, J. X., et al. 2009, ApJS, 185, 526, doi: 10.1088/0067-0049/185/2/526

Gehrels, N., Ramirez-Ruiz, E., & Fox, D. B. 2009, ARA&A, 47, 567, doi: 10.1146/annurev.astro.46.060407.145147

Gehrels, N., Chincarini, G., Giommi, P., et al. 2004, ApJ, 611, 1005, doi: 10.1086/422091

Graham, M. J., Kulkarni, S. R., Bellm, E. C., et al. 2019, PASP, 131, 078001, doi: 10.1088/1538-3873/ab006c

Granot, J., & Piran, T. 2012, MNRAS, 421, 570, doi: 10.1111/j.1365-2966.2011.20335.x

Greiner, J., Krühler, T., Klose, S., et al. 2011, A&A, 526, A30, doi: 10.1051/0004-6361/201015458

Hamburg, R., & Fermi-GBM Team. 2020, GRB Coordinates Network, 26970, 1

Harrison, F. A., Yost, S. A., Sari, R., et al. 2001, arXiv e-prints, astro. https://arxiv.org/abs/astro-ph/0103377

Hjorth, J., Malesani, D., Jakobsson, P., et al. 2012, ApJ, 756, 187, doi: 10.1088/0004-637X/756/2/187

Ho, A. Y. Q., Yao, Y., Perley, D. A., & GROWTH Collaboration. 2020, GRB Coordinates Network, 25658, 1

Ho, A. Y. Q., Kulkarni, S. R., Nugent, P. E., et al. 2018, ApJL, 854, L13, doi: 10.3847/2041-8213/aaaa62

Ho, Y. Q., Cenko, S. B., Perley, D. A., & GROWTH Collaboration. 2019, GRB Coordinates Network, 25658, 1

Högbom, J. A. 1974, A&AS, 15, 417

Hook, I. M., Jørgensen, I., Allington-Smith, J. R., et al. 2004, PASP, 116, 425, doi: 10.1086/383624

Jones, F. C., & Ellison, D. C. 1991, SSRv, 58, 259, doi: 10.1007/BF01206003

Kann, D. A., Klose, S., Zhang, B., et al. 2010, ApJ, 720, 1513, doi: 10.1088/0004-637X/720/2/1513

Kasliwal, M. M., Cannella, C., Bagdasaryan, A., et al. 2019, PASP, 131, 038003, doi: 10.1088/1538-3873/aafbc2

Klose, S., Greiner, J., Rau, A., et al. 2004, AJ, 128, 1942, doi: 10.1086/424539

Kocevski, D., & Butler, N. 2008, ApJ, 680, 531, doi: 10.1086/586693

Kouveliotou, C., Wijers, R. A. M. J., & Woosley, S. 2012, Gamma-ray Bursts

Kowalski, A. F., Hawley, S. L., Wisniewski, J. P., et al. 2013, ApJS, 207, 15, doi: 10.1088/0067-0049/207/1/15

Kulkarni, S. R., & Rau, A. 2006, ApJL, 644, L63, doi: 10.1086/505423

Kulkarni, S. R., Djorgovski, S. G., Odewahn, S. C., et al. 1999, Nature, 398, 389, doi: 10.1038/18821

Kumar, P., & Zhang, B. 2015, PhR, 561, 1, doi: 10.1016/j.physrep.2014.09.008

Laskar, T., Berger, E., Zauderer, B. A., et al. 2013, ApJ, 776, 119, doi: 10.1088/0004-637X/776/2/119

Laskar, T., Alexander, K. D., Berger, E., et al.
2016, ApJ, 833, 88,
doi: 10.3847/1538-4357/833/1/88

Laskar, T., Berger, E., Margutti, R., et al. 2018,
ApJ, 859, 134, doi: 10.3847/1538-4357/aabfd8

Law, N. M., Kulkarni, S. R., Dekany, R. G., et al.
2009, PASP, 121, 1395, doi: 10.1086/648598

Liang, E.-W., Racusin, J. L., Zhang, B., Zhang,
B.-B., & Burrows, D. N. 2008, ApJ, 675, 528,
doi: 10.1086/524701

Lien, A., Sakamoto, T., Gehrels, N., et al. 2014,
ApJ, 783, 24, doi: 10.1088/0004-637X/783/1/24

MacFadyen, A. I., & Woosley, S. E. 1999, ApJ,
524, 262, doi: 10.1086/307790

Mahabal, A. A., Djorgovski, S. G., Drake, A. J.,
et al. 2011, Bulletin of the Astronomical Society
of India, 39, 387.
https://arxiv.org/abs/1111.0313

Masci, F. J., Laher, R. R., Rusholme, B., et al.
2019, PASP, 131, 018003,
doi: 10.1088/1538-3873/aae8ac

McMullin, J. P., Waters, B., Schiebel, D., Young,
W., & Golap, K. 2007, Astronomical Society of
the Pacific Conference Series, Vol. 376, CASA
Architecture and Applications, ed. R. A. Shaw,
F. Hill, & D. J. Bell, 127

Meegan, C., Lichti, G., Bhat, P. N., et al. 2009,
ApJ, 702, 791,
doi: 10.1088/0004-637X/702/1/791

Mészáros, P. 2006, Reports on Progress in Physics,
69, 2259, doi: 10.1088/0034-4885/69/8/R01

Mészáros, P., & Rees, M. J. 1997, ApJL, 482, L29,
doi: 10.1086/310692

—. 1999, MNRAS, 306, L39,
doi: 10.1046/j.1365-8711.1999.02800.x

Mészáros, P., Rees, M. J., & Wijers, R. A. M. J.
1998, ApJ, 499, 301, doi: 10.1086/305635

Nakar, E., & Piran, T. 2003, NewA, 8, 141,
doi: 10.1016/S1384-1076(02)00202-6

Nysewander, M., Fruchter, A. S., & Pe'er, A.
2009, ApJ, 701, 824,
doi: 10.1088/0004-637X/701/1/824

Oke, J. B., Cohen, J. G., Carr, M., et al. 1995,
PASP, 107, 375, doi: 10.1086/133562

Panaitescu, A., & Kumar, P. 2001, ApJL, 560,
L49, doi: 10.1086/324061

—. 2002, ApJ, 571, 779, doi: 10.1086/340094

Panaitescu, A., Mészáros, P., & Rees, M. J. 1998,
ApJ, 503, 314, doi: 10.1086/305995

Patterson, M. T., Bellm, E. C., Rusholme, B.,
et al. 2019, PASP, 131, 018001,
doi: 10.1088/1538-3873/aae904

Perley, D. A. 2019, PASP, 131, 084503,
doi: 10.1088/1538-3873/ab215d

Perley, D. A., Cenko, S. B., Corsi, A., et al. 2014,
ApJ, 781, 37, doi: 10.1088/0004-637X/781/1/37

Perley, R. A., Chandler, C. J., Butler, B. J., &
Wrobel, J. M. 2011, ApJL, 739, L1,
doi: 10.1088/2041-8205/739/1/L1

Piran, T. 2004, Reviews of Modern Physics, 76,
1143, doi: 10.1103/RevModPhys.76.1143

Planck Collaboration, Ade, P. A. R., Aghanim,
N., et al. 2016, A&A, 594, A13,
doi: 10.1051/0004-6361/201525830

Ramirez-Ruiz, E., Granot, J., Kouveliotou, C.,
et al. 2005, ApJL, 625, L91, doi: 10.1086/431237

Rau, A., Ofek, E. O., Kulkarni, S. R., et al. 2008,
ApJ, 682, 1205, doi: 10.1086/589762

Rhoads, J. E. 1997, ApJL, 487, L1,
doi: 10.1086/310876

Ridnaia, A., Golenetskii, S., Aptekar, R., et al.
2020, GRB Coordinates Network, 27039, 1

Rigault, M., Neill, J. D., Blagorodnova, N., et al.
2019, A&A, 627, A115,
doi: 10.1051/0004-6361/201935344

Ryan, G., van Eerten, H., Piro, L., & Troja, E.
2019, arXiv e-prints, arXiv:1909.11691.
https://arxiv.org/abs/1909.11691

Sari, R., Piran, T., & Halpern, J. P. 1999, ApJL,
519, L17, doi: 10.1086/312109

Sari, R., Piran, T., & Narayan, R. 1998, ApJL,
497, L17, doi: 10.1086/311269

Schlafly, E. F., & Finkbeiner, D. P. 2011, ApJ,
737, 103, doi: 10.1088/0004-637X/737/2/103

Selsing, J., Malesani, D., Goldoni, P., et al. 2019,
A&A, 623, A92,
doi: 10.1051/0004-6361/201832835

Singer, L. P., Ahumada, T., Ho, A. Y. Q., ZTF, &
GROWTH Collaboration. 2020, GRB
Coordinates Network, 26968, 1

Stalder, B., Tonry, J., Smartt, S. J., et al. 2017,
ApJ, 850, 149, doi: 10.3847/1538-4357/aa95c1

Steele, I. A., Smith, R. J., Rees, P. C., et al. 2004,
in Proc. SPIE, Vol. 5489, Ground-based
Telescopes, ed. J. M. Oschmann, Jr., 679–692,
doi: 10.1117/12.551456

Tachibana, Y., & Miller, A. A. 2018, PASP, 130,
128001, doi: 10.1088/1538-3873/aae3d9

van Eerten, H. J., Meliani, Z., Wijers, R. A. M. J., & Keppens, R. 2011, MNRAS, 410, 2016, doi: 10.1111/j.1365-2966.2010.17582.x

van Paradijs, J., Kouveliotou, C., & Wijers, R. A. M. J. 2000, ARA&A, 38, 379, doi: 10.1146/annurev.astro.38.1.379

van Roestel, J., Groot, P. J., Kupfer, T., et al. 2019, MNRAS, 484, 4507, doi: 10.1093/mnras/stz241

Wang, X.-G., Zhang, B., Liang, E.-W., et al. 2018, ApJ, 859, 160, doi: 10.3847/1538-4357/aabc13

Yao, Y., Miller, A. A., Kulkarni, S. R., et al. 2019, ApJ, 886, 152, doi: 10.3847/1538-4357/ab4cf5

Yaron, O., & Gal-Yam, A. 2012, PASP, 124, 668, doi: 10.1086/666656

Zackay, B., Ofek, E. O., & Gal-Yam, A. 2016, ApJ, 830, 27, doi: 10.3847/0004-637X/830/1/27

Zeh, A., Klose, S., & Kann, D. A. 2006, ApJ, 637, 889, doi: 10.1086/498442

Zhang, B., & Mészáros, P. 2004, International Journal of Modern Physics A, 19, 2385, doi: 10.1142/S0217751X0401746X

Zhang, B.-B., van Eerten, H., Burrows, D. N., et al. 2015, ApJ, 806, 15, doi: 10.1088/0004-637X/806/1/15